ELSEVIER

Inorganica Chimica Acta 227 (1994) 33–41

Inorganica Chimica Acta

One-equivalent oxidative charge storage on an $[Mn_2O_2]^{3+}$ core: synthesis, crystal structure and resonance Raman spectra of $[Mn_2O_2(pbz)_4]^{n+}$ $(n=3,\ 4)$

Bakul C. Dave, Roman S. Czernuszewicz *

Department of Chemistry, University of Houston, Houston, TX 77204, USA

Received 11 January 1994; revised 11 May 1994

Abstract

Complexes similar in structure but with a higher oxidation state of the metal center mimic charge-storage processes observed in biological systems. An oxomanganese system based on the ligand 2(2′-pyridyl)benzimidazole, $[Mn_2O_2(pbz)_4]^{3+}$, which contains the biologically relevant mixed-valent di-μ-oxo Mn(III,IV) unit capable of undergoing a pH controlled one-electron redox conversion to the Mn(IV,IV) state, is described. The $[Mn_2O_2(pbz)_4]^{4+}$ and $[Mn_2O_2(pbz)_4]^{3+}$ complexes have both been isolated and structurally characterized by X-ray crystallography and UV–Vis, EPR and resonance Raman spectroscopic methods. A characteristic Mn(IV)–O stretching mode of the (di-μ-oxo)dimanganese core in these complexes at ~ 695 cm^{-1} provides a useful reference probe for structural characterization of Mn containing active sites involving two oxo bridges.

Keywords: Crystal structures; Manganese complexes; Oxo complexes

1. Introduction

The study of high-valent manganese complexes with bridging oxide ligands is becoming increasingly important due to the potential involvement of μ-oxo-bridged cores at the active sites of manganese containing enzymes [1]. The primary function of Mn centers in biology appears to be oxidation–reduction stemming from a facile accessibility of various oxidation states of the Mn atom at biologically attainable conditions. A dinuclear Mn site is found to be involved in a two-electron catalytic disproportionation of peroxide to water and dioxygen in non-heme bacterial catalases [2], whereas it is commonly believed that a tetranuclear Mn oxo aggregate is involved in a four-electron, light-driven oxidation of water to dioxygen at the oxygen evolving center (OEC) of the green plant photosystem II (PSII) [3]. The OEC achieves its function by five readily accessible states, called the S states (S_0–S_4) [4], which involve proton ionizations between $S_0 \rightarrow S_1$, $S_2 \rightarrow S_3$ and $S_3 \rightarrow [S_4] \rightarrow S_0$ [5]. The S_2 state has been found to show a multiline EPR signal centered at $g=2$ [6]. Similar multiline signals due to ^{55}Mn hyperfine coupling have also been observed for the superoxidized Mn(III,IV) form of catalases [2d]. To a first approximation, the EXAFS spectra of superoxidized catalase and OEC in the S_2 state also look very much alike in that they both show an Mn–Mn interaction at ~ 2.7 Å [2f]. These EPR and EXAFS features are characteristic of the di-μ-oxo dimanganese core in Mn(III,IV) (EPR, EXAFS) and Mn(IV,IV) (EXAFS) oxidation states, suggesting a similarity in sub-structure between the two enzymes. Understanding the factors which control the delicate balance between oxidation states of the basic dimanganese units and their transformations in aqueous medium continue to be an important issue in deeper understanding of these fascinating biological systems.

The chemical approach to gain an insight into the S state advancement in OEC, and accompanying charge storage steps, involves achieving the experimental conditions under which a variety of complexes in different oxidation states can be isolated, especially with the same ligation and the nuclearity unchanged to delineate the factors which lead to stabilization of additional

Abbreviations used: pbz, 2(2-pyridyl)benzimidazole; bpy, 2,2′-bipyridine; phen, 1,10-phenanthroline; tpen, *N,N,N′,N′*-tetrakis(2-pyridylmethyl)-1,3-ethanediamine; bpea, *N,N*-bis(2-pyridyl-methyl)-ethylamine; saltn, 1,3-bis(salicylideneiminato)propane; PSII, photosystem II; OEC, oxygen evolving center; IR, infrared; RR, resonance Raman; EPR, electron paramagnetic resonance; EXAFS, extended X-ray absorption fine structure; SCE, saturated calomel electrode.

*Corresponding author.

SSDI 0020-1693(94)04128-I

charge equivalents on the cluster. Complexes similar in structure but with a higher oxidation state of the metal center model the charge-storage process observed in the biological system. With this in mind, we have recently demonstrated that the μ-oxo-di-μ-acetato Mn(III,III) complex, $[Mn_2O(O_2CCH_3)_2(bpy)_4]^{2+}$, previously synthesized and structurally characterized by Girerd and co-workers [7], can undergo a proton-induced, two-electron oxidation upon addition of perchloric acid to form a di-μ-oxo-μ-carboxylato bridged Mn(IV,IV) dimer, $[Mn_2O_2(O_2CCH_3)(bpy)_4]^{3+}$, while retaining one of its bridging acetates and both terminally ligated water molecules [8]. In addition, there have been numerous studies conducted on the dinuclear Mn complexes possessing a mixed-valent $[Mn_2(\mu\text{-}O)_2]^{3+}$ core that have established proton-coupled electron transfer in their redox transformations as well [9]. For example, these complexes are reduced to the Mn(III,III) oxidation state under electrochemical conditions [9]. Under self-assembly conditions, however, the $[Mn_2(\mu\text{-}O)_2]^{3+}$ cores undergo facile transformations to Mn(IV) containing clusters of varying metal nuclearities depending on the pH of the reacting solution and the coordinated ligands. Thus, the di-μ-oxo-μ-carboxylato bridged dimanganese(III,IV) units with tridentate ligands such as bpea and tpen disproportionate in acidic aqueous medium to form their corresponding Mn(IV,IV) dimers, but at higher pH are converted to the (IV,IV,IV) trimers possessing the $[Mn_3(\mu\text{-}O)_4]^{4+}$ core [10].

In contrast, the classical $[Mn_2O_2(bpy)_4]^{3+}$ cation [11], which lacks the carboxylato bridging moiety, is readily disproportionated to the trinuclear $[Mn_3O_4(H_2O)_2(bpy)_4]^{4+}$ species as the main product even in very acidic conditions [12]. In this work, we report the system based on the ligand 2(2′-pyridyl)benzimidazole (pbz), $[Mn_2O_2(pbz)_4]^{3+}$ (**1**), which contains the biologically relevant mixed-valent di-μ-oxo Mn(III,IV) unit capable of undergoing a pH controlled quasi-reversible one-electron oxidation to the Mn(IV,IV) state without significant structural changes. The Mn(IV,IV) complex $[Mn_2O_2(pbz)_4]^{4+}$ (**2**), as well as its one-electron reduced starting material $[Mn_2O_2(pbz)_4]^{3+}$ (**1**), have been isolated and structurally characterized by X-ray crystallography, UV–Vis, EPR and resonance Raman spectroscopic methods.

2. Materials and methods

2.1. Synthesis of the complexes

All the chemicals used were of reagent grade. $Mn(O_2CCH_3)_2\cdot 4H_2O$, $KMnO_4$ and 2(2′-pyridyl)-benzimidazole (pbz) were purchased from Aldrich Chemical Co. (Milwaukee, WI) and were used as received. All the solvents were used without further purification. Elemental analyses were performed by Texas Analytical Lab, Houston, TX.

2.1.1. $[Mn_2O_2(pbz)_4](ClO_4)_3\cdot H_2O$ (1)

The synthesis of mixed-valent $[(pbz)_2Mn^{III}(\mu\text{-}O)_2Mn^{IV}(pbz)_2]^{3+}$ (**1**) was carried out in a manner similar to that for the bpy Mn(III,IV) dimer [11b]. To a solution containing 0.43 g (1.75 mmol) of $Mn(O_2CCH_3)_2\cdot 4H_2O$ in 25 ml of water were added 5 ml of glacial acetic acid, followed by addition of 1.024 g (5.24 mmol) of the pbz ligand in 30 ml of methanol to give an orange–brown solution. To this orange–brown mixture was added 0.118 g (0.75 mmol) of $KMnO_4$ in 20 ml of water to produce a green–brown solution from which **1** was precipitated by adding 3.0 g of $NaClO_4$. Yield 0.97 g (62% based on total Mn). Single crystals suitable for X-ray analysis were obtained by recrystallization from acetonitrile. *Anal.* Calc. for $C_{48}H_{38}N_{12}O_{15}Mn_2Cl_3$: C, 46.48; H, 3.31; N, 13.55. Found: C, 46.37; H, 2.79; N, 13.47%.

2.1.2. $[Mn_2O_2(pbz)_4](ClO_4)_4\cdot 4H_2O$ (2)

$[(pbz)_2Mn^{IV}(\mu\text{-}O)_2Mn^{IV}(pbz)_2]^{4+}$ (**2**) was prepared by in situ disproportionation of **1** with perchloric acid. First, the green–brown solution containing **1** was obtained as described above. Addition of 10 ml of concentrated $HClO_4$ (~70%) to the green–brown solution resulted in precipitation of the red–brown colored **2**. The synthesis of complex **2** can also be achieved by using a pre-isolated compound **1**, by dissolving it in acetonitrile followed by treatment with concentrated $HClO_4$. In both cases, there was co-precipitation of a white impurity, and therefore, the exact yields of the reaction were difficult to determine. **Caution!** Perchloric acid and its salts are all potentially explosive and should be handled with care. Good X-ray quality single crystals of **2** were obtained by recrystallization from a 1:1 mixture of acetone and acetonitrile. *Anal.* Calc. for $C_{48}H_{44}N_{12}O_{22}Mn_2Cl_4$: C, 41.35; H, 3.41; N, 12.06; Mn, 7.89. Found: C, 41.32; H, 3.08; N, 12.01; Mn, 8.06%.

2.2. X-ray structure determination

The crystal structures were determined on a Nicolet R3m/V automatic diffractometer. The radiation used was Mo Kα monochromatized by a highly ordered graphite crystal. Intensities were measured using the ω scan technique, with the scan rate depending on the count obtained in rapid pre-scans of each reflection. Two standard reflections were monitored after every two hours or after every 100 data collected, and these showed no significant change during the course of the experiment. During data reduction Lorentz and polarization corrections were applied, however, no correction for absorption was made due to the small

absorption coefficients. All calculations were made using Nicolet's SHELXTL PLUS (1987) series of crystallographic programs.

2.2.1. $[Mn_2O_2(pbz)_4](ClO_4)_3 \cdot H_2O$ (1)

A black, square column of **1** having approximate dimensions $0.40 \times 0.12 \times 0.10$ mm was cut from one finger of a feather shaped multiple crystal and mounted on the diffractometer. The Laue symmetry was determined to be $4/m$, and from the systematic absences noted, the space group was shown to be either $P4_1$ or $P4_3$. Final cell constants as well as other information pertinent to data collection and refinement are given in Table 1. The structure was solved by use of the SHELXTL direct methods program, which revealed most of the atoms in the molecule. Remaining non-hydrogen atoms were located in subsequent difference Fourier syntheses. Due to the relatively small amount of observed data, only the Mn and N atoms were refined anisotropically. Carbons were refined isotropically. All hydrogen atoms were entered in ideal calculated positions and constrained to riding motion, with a single variable isotropic temperature factor for all of them. The hydrogens on the solvent water molecule could not be located. Two of the three perchlorate anions are disordered, both having two orientations. These two anions (Cl1 and Cl2) were refined as rigid bodies, with population factors of 55%:45% for Cl1:Cl1′ and the same ratio for Cl2:Cl2′. The absolute configuration of the cation was determined by refinement of a variable which multiplies $\Delta f''$ (Rogers test), and the results indicated strongly that the reported structure in space group $P4_3$ is preferred over the opposite configuration in space group $P4_1$. After all shift/e.s.d. ratios were less than 0.1 (excepting hydrogens), convergence was reached at the agreement factors listed in Table 1. No unusually high correlations were noted in the last cycle of full-matrix least-squares refinement, and the final difference density map showed a maximum peak of about 0.4 e $Å^{-3}$.

2.2.2. $[Mn_2O_2(pbz)_4](ClO_4)_4 \cdot 4H_2O$ (2)

A dark burgundy colored parallelepiped of **2** having approximate dimensions of $0.30 \times 0.25 \times 0.20$ mm was used for data collection. The Laue symmetry was determined to be $2/m$, and from the systematic absences noted the space group was shown to be either Pn or $P2/n$. Since the unitary structure factors displayed centric statistics, space group $P2/n$ was assumed from the outset. Final cell constants as well as other information pertinent to data collection and refinement are listed in Table 1. The structure was solved by interpretation of the Patterson map, which revealed the positions of the Mn atoms in the asymmetric unit, consisting of one-half cation situated about a two-fold axis and two anions in general positions. The usual sequence of isotropic and anisotropic refinement was followed, after which all hydrogens were entered in ideal calculated positions and constrained to riding motion, with a single variable isotropic temperature factor for all of them. Two independent water molecules of solvation were found in the asymmetric unit, and these were treated as ideal

Table 1
Crystallographic data for $[Mn_2O_2(pbz)_4](ClO_4)_3 \cdot H_2O$ (1) and $[Mn_2O_2(pbz)_4](ClO_4)_4 \cdot 4H_2O$ (2)

	1, Mn(III,IV)	2, Mn(IV,IV)
Formula	$Mn_2O_{15}C_{48}H_{38}N_{12}Cl_3$	$Mn_2O_{22}C_{48}H_{44}N_{12}Cl_4$
Formula weight	1239.21	1392.72
Crystal system	tetragonal	monoclinic
Space group	$P4_3$	$P2/n$
Temperature (K)	298	298
a (Å)	13.042(4)	13.299(2)
b (Å)		14.700(3)
c (Å)	29.785(11)	14.803(3)
β (°)		96.21(1)
V ($Å^3$)	5066	2877
Z	4	2
Crystal dimensions (mm)	$0.40 \times 0.12 \times 0.10$	$0.30 \times 0.25 \times 0.20$
Crystal density (g cm^{-3})	1.62	1.61
Absorption coefficient (cm^{-1})	7.17	6.94
Radiation, Mo Kα (Å)	0.71073	0.71073
2θ Limits (°)	4–45	4–45
Scan width, $\Delta\theta$ (°)	$1.20 + (K\alpha_2 - K\alpha_1)$	$1.20 + (K\alpha_2 - K\alpha_1)$
Scan speed (°/min)	1.5–15.0	1.5–15.0
Total data collected	3358	3771
Independent data, $I > 3\sigma(I)$	1897	2484
Total variables	389	374
R, R_w[a]	0.060, 0.043	0.059, 0.048

[a] $R = \Sigma\|\|F_o\| - |F_c\|\|/\Sigma|F_o|$; $R_w = [\Sigma w(\|F_o| - |F_c|)^2/\Sigma w|F_o|^2]^{1/2}$; $w = \sigma(F)^{-2}$.

rigid bodies and allowed to rotate freely. One of the two anions was found to be disordered, having two different orientations centered roughly about the same position. This was treated as two ideal rigid bodies, and based on analysis of the isotropic temperature factors involved the population factors assigned were 55% for the Cl2 group and 45% for the Cl2′ group. After all shift/e.s.d. ratios were less than 0.1, convergence was reached at the agreement factors listed in Table 1. No unusually high correlations were noted in the last cycle of full-matrix least-squares refinement, and the final difference density map showed a maximum peak of about 0.6 e $Å^{-3}$.

2.3. Spectroscopic measurements

Resonance Raman spectra were obtained by excitation with 457.9 and 488.0 nm lines from a Coherent 90-6 Ar^+ ion laser. The ^{18}O-substituted **1** and **2** were prepared by equilibrating millimolar samples dissolved in CH_3CN solutions (2 ml) with ~50 μl of pure $H_2{}^{18}O$ water (97–99 at.% ^{18}O, Cambridge Isotope Laboratories, Woburn, MA) for half an hour followed by complete evaporation to dryness of the solvent under a nitrogen stream. The scattered photons were collected via back-scattering geometry from spinning solid samples in pressed KCl pellets [13a]. A scanning Raman instrument equipped with a Spex 1403 double monochromator and a Hamamatsu 928 photomultiplier detector system was used to record the spectra under the control of a Spex DM3000 microcomputer system, as described in detail elsewhere [13b]. An average of multiple scans (8–10) was taken to improve signal to noise ratio. Raman data manipulation was performed using LabCalc software (Galactic Industries Inc.) on a 486-DX 33 MHz PC microcomputer. Baseline correction was performed utilizing the two-point baseline correction LabCalc routine. A Hewlett-Packard 8-pen ColorPro graphics plotter was used to hardcopy output of spectra.

Absorption spectra were obtained on an HP-8542 diode array spectrophotometer in 1 mm quartz cuvettes using acetonitrile as a solvent. The pH dependence was monitored by using 2 ml of 0.05 M solution of **1** in acetonitrile. Successive aliquots (20 μl) of ~10% $HClO_4$ were added till no increase in the intensity of the 515 nm band was observed. Thereafter, 20 μl aliquots of 0.1 M NaOH solution were added till the precipitation of MnO_2 was encountered.

Magnetic moments were obtained in the laboratory of Dr C.J. Carrano at Southwest Texas State University using a Faraday balance attached to a liquid helium cryostat. The EPR spectra of **1** and **2** were kindly measured by Dr G.C. Dismukes at Princeton University.

3. Results and discussion

3.1. pH controlled conversion of the $[Mn_2O_2]^{3+}$ core to the $[Mn_2O_2]^{4+}$ core

Shown in Fig. 1 are the absorption spectra obtained on successive addition of perchloric acid to an acetonitrile solution of **1** (0.05 M). The addition of small aliquots (20 μl) of $HClO_4$ causes a systematic increase in the peak at 515 nm (spectra 1–5). After saturation is reached, addition of NaOH leads to a decrease in the intensity (spectra 6–8). The solution thus treated (spectrum 8), however, regains most of its absorption at 515 nm upon subsequent addition of $HClO_4$, which diminishes again when more base is mixed in. This cycle can be repeated qualitatively several times as long as not too much NaOH is added in the steps preceding the addition of $HClO_4$. This demonstrates that addition of perchloric acid leads to the formation of a new complex with an absorption at 515 nm, which converts back to **1** in the presence of OH^- and then gets regenerated with a fresh portion of $HClO_4$, albeit the reaction is not completely reversible.

In acidic media, it has been shown that the oxo bridges could be protonated in the cases of Fe [14a], V [14b,c] and Mn [15]. The structural characterization of the product isolated on acidification of the Mn(III,IV) complex **1** (vide infra) showed the presence of a di-manganese core with an overall +4 charge, which is consistent with the oxidation state formulation as: $Mn^{III}(\mu\text{-OH})(\mu\text{-OH})Mn^{III}$, $Mn^{III}(\mu\text{-OH})(\mu\text{-O})Mn^{IV}$ or $Mn^{IV}(\mu\text{-O})_2Mn^{IV}$. Due to the inability of the X-ray experiment to locate the protons, it was not possible to determine if the changes in the UV–Vis absorption spectra were due to a protonation of the oxo bridge(s) or the formation of the di-μ-oxo Mn(IV,IV) complex.

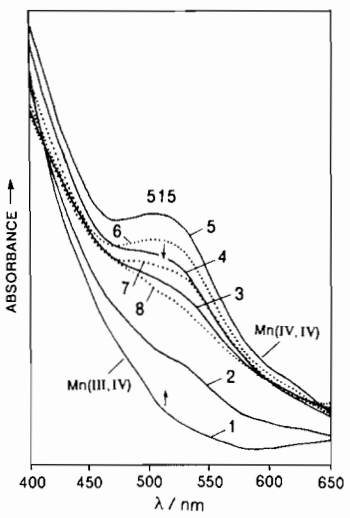

Fig. 1. Changes in the UV–Vis absorption spectrum of $[Mn_2O_2(pbz)_4]^{3+}$ (**1**) upon addition of $HClO_4$ (spectra 1–5) followed by addition of NaOH (spectra 6–8). (see Section 2 for details.)

However, in oxo-bridged complexes there is a partial double bond character to the M–O bonds due to substantial π-bonding between the oxo atom and the metal d-orbitals. Protonation causes the hybridization of the μ-oxo atom to change, and the M–OH distances are considerably longer ($\sim$0.1 Å) than the M–O distances. The close similarity of the structural parameters of **2** (see Table 2) with those of the well-characterized phenanthroline di-μ-oxo Mn(IV,IV) dimer, $[Mn_2O_2(phen)_4]^{4+}$ [16], rules out the possibility of the protonation of an oxo bridge due to acidification. Also, the structural parameters of **1** and **2** do not conform to those of $[Mn_2O_2(saltn)_2]$ (saltn = 1,3-bis(salicylideneiminato)propane), which has been shown to contain a monoprotonated Mn_2O_2 core upon addition of acid with Mn–O and Mn–Mn distances of about 0.1 Å longer than the unprotonated dimer [15b]. In the case of the saltn ligand the protonation of the oxo bridge was ascribed to the anionic charge and stronger electron-donating capability of the phenolato groups. In complex **2**, the poorer donor properties of the pyridyl and imidazolyl nitrogens of pbz leave the high-valent Mn atoms sufficiently formally charged to interact with the π-orbitals of the oxo atoms, thus preventing any additional bonding interactions by the bridging oxo groups with a proton.

The formation of **2** from acidification of **1** can be rationalized by assuming a pH induced disproportionation of the $[Mn_2O_2]^{3+}$ core to give an $[Mn_2O_2]^{4+}$-containing dimer and a μ-hydroxo-μ-oxodimanganese(III,III) species which, due to the inability of an all N-donor ligating environment to support the (III,III) oxidation state, undergoes decomposition to an Mn^{2+} species (Scheme 1(a)). It seems also plausible that initial protonation of the di-μ-oxo bridge simply raises the dimer's redox potential, thus allowing it to oxidize the unprotonated dimer (Scheme 1(b)). The transformation of **1** to **2** was carried out aerobically and the potential involvement of a pH induced air oxidation cannot be ruled out either. We note that in the absence of mechanistic studies the nature of the actual steps will be difficult to define. However, observation of the Mn^{2+} signal in the EPR spectrum of **2** supports the acid induced disproportionation pathway.

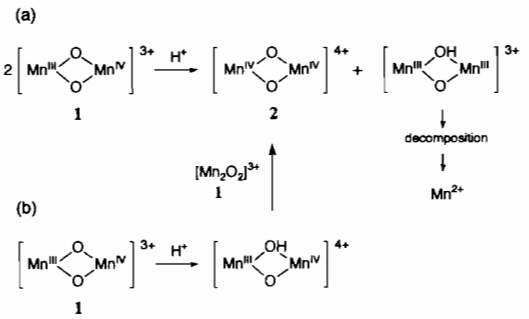

Scheme 1.

Formation of the Mn(IV,IV) complex from a solution containing the Mn(III,IV) core indicates a disproportionation pathway via an outer-sphere intermolecular electron transfer process. Since oxo bridges have the shortest bonds in the *xy* plane, the approximate relative ordering of the Mn orbitals for the Mn_2O_2 core can be given as $d_{x^2-y^2} > d_{z^2} > d_{xy} > d_{xz}$, d_{yz}. According to this scheme, the Mn(III,IV) to Mn(IV,IV) transformation involves the removal of an electron from the d_{z^2} orbital. As a consequence, only the bond lengths of the Mn–N bonds *cis* to the oxo group (along the *z* axis) are expected to undergo a change during the intermolecular redox process. Indeed, for the crystallographically characterized Mn(III,IV) and Mn(IV,IV) analogs of **1** and **2** with the phen ligand, the average $Mn–N_{cis}$ bond length changes from 2.127(3) to 2.010(3) Å, respectively (difference, $\Delta = 0.117(3)$ Å), whereas the $Mn–N_{trans}$ ($\Delta = 0.029(3)$ Å) and Mn–O ($\Delta = 0.012(3)$ Å) bond distances are relatively unaltered [16]. This change of $Mn–N_{cis}$ bond distance lies along the Jahn–Teller distortion axis for d^4 Mn(III), and is therefore energetically favored due to a reduction of activation energy on going from Mn(IV) to Mn(III). The oxidation pathway involves the formation of Mn(IV) with a half-filled t_{2g} shell. These two factors should be the driving influence towards an intermolecular electron transfer causing disproportionation of the mixed-valent Mn(III,IV) unit in **1**, in spite of the nearly unchanged $Mn–N_{cis}$ bond lengths for **1** and **2** (vide infra). The absence of a similar chemistry with bpy [12] may be due to the higher basicity of the bpy ligand that leads to a protonation of the ligand resulting in loss of coordination, with a subsequent structural rearrangement to give rise to the $[Mn_3O_4]^{4+}$ trimer.

3.2. Crystal structures of 1 and 2

Both the crystals were subjected to X-ray analysis, however, partly due to the poor quality of crystals obtained for **1** and partly due to disorder of the ClO_4^- anions, the resolution for **1** was not up to the level which could allow a detailed comparison with the structural parameters obtained for **2**. Nevertheless, the X-ray crystal crystallography of **1** showed an agreement with the molecular formula consistent with elemental analysis. The molecular formulas for **1** and **2** were determined to be $[Mn_2O_2(pbz)_4](ClO_4)_3 \cdot H_2O$ and $[Mn_2O_2(pbz)_4](ClO_4)_4 \cdot 4H_2O$, respectively. The ORTEP drawings and atom labeling schemes are presented in Fig. 2 for **1** and Fig. 3 for **2**, while selected interatomic distances and bond angles for **1** and **2** are given in Tables 2 and 3, respectively.

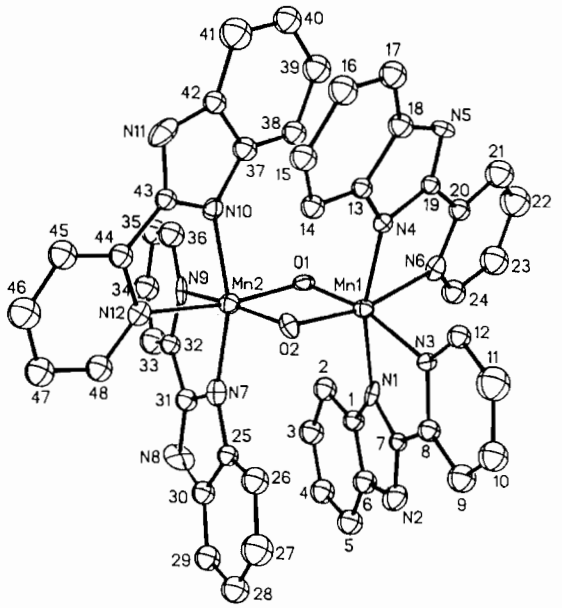

Fig. 2. ORTEP drawing of $[Mn_2O_2(pbz)_4]^{3+}$ (**1**) showing the crystal structure and atom labeling scheme. The bond lengths and bond angles are listed in Table 2.

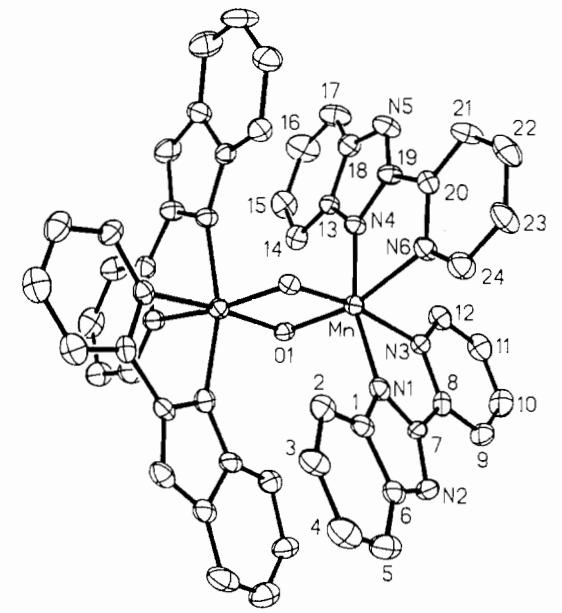

Fig. 3. ORTEP drawing of $[Mn_2O_2(pbz)_4]^{4+}$ (**2**) showing the crystal structure and atom labeling scheme. The bond lengths and bond angles are listed in Table 3.

3.2.1. $[Mn_2O_2(pbz)_4](ClO_4)_3 \cdot H_2O$ (1)

The mixed-valent Mn(III,IV) complex **1** crystallizes in the tetragonal $P4_3$ space group with cell constants $a = 13.0042(3)$, $c = 29.785(3)$ Å and $V = 5066$ Å^3, and four molecules per unit cell. The structure of **1** shows a distorted octahedral environment about each Mn atom (Fig. 2). The four ligands bind with the pyridyl nitrogens *trans* to the bridging oxygens. The four-membered Mn_2O_2 ring is not quite planar; the two O–Mn–O planes subtend an angle of 5.4° which results in a shorter O···O distance (2.345 Å) as compared to those in the corresponding bpy (2.419 Å) [11a] and phen (2.425 Å) [16] mixed-valent Mn(III,IV) complexes. The Mn–N_{pyr} bonds (av. 2.10 Å) are significantly longer than the Mn–N_{aza} bonds (av. 1.98 Å).

3.2.2. $[Mn_2O_2(pbz)_4](ClO_4)_4 \cdot 4H_2O$ (2)

On the other hand, the high-valent Mn(IV,IV) complex **2** crystallizes in the monoclinic $P2/n$ space group with cell constants $a = 13.299(2)$, $b = 14.700(3)$, $c = 14.803(3)$ Å, $\beta = 96.21(1)°$ and $V = 2877$ Å^3, and two molecules per unit cell. The molecular structure of **2** shows a crystallographically imposed C_2 axis of symmetry with a totally symmetric $[Mn_2O_2]^{4+}$ core (Fig. 3). The average Mn–O bond length is 1.798(4) Å which compares well with the value of 1.799(2) Å observed for the analogous complex with phen ligand [16]. The pbz ligands are slightly distorted from planarity, with the torsion angles across the chelating N–C–C–N bites being −4.5° and 5.9°. The average bond length of nitrogens *trans* to the oxo bridges (N_{pyr}) is considerably longer than that of the *cis* nitrogens (N_{aza}), 2.100(6) and 1.968(6) Å, respectively. This implies a structural *trans* effect of the oxo bridges. Since the oxo atoms define the *xy* plane in the di-μ-oxo complex for Mn(IV), a d^3 system, the most stable coordinating environment is obtained with the strongly donating ligands occupying the *xy* plane *trans* to the oxo bridges, which for pbz are the pyridyl nitrogens.

3.3. Physical measurements

The EPR spectrum of **1** in acetonitrile at 110 K, presented in Fig. 4, shows a 16-line signal with ^{55}Mn hyperfine structure centered at $g = 2$ characteristic of an antiferromagnetically coupled ($S = 1/2$ ground state) Mn(III,IV) dimer. This signal, which has parameters essentially identical to those calculated for the bpy analog, $[Mn_2O_2(bpy)_4]^{3+}$ [11c], confirms the valencc trapped nature of the complex. As expected, complex **2** is EPR silent, although weak signals due to small amounts of **1** and Mn(II) species were detected in the bulk crystalline samples. The UV–Vis absorption spectrum of **1** in acetonitrile, which displayed poorly resolved shoulders at ~525, 555 and 685 nm, was found to be similar to the ones obtained for bpy and phen Mn(III,IV) dimers [11b], implying that the origin of the spectrum is due to the $[Mn_2O_2]^{3+}$ core only and is not perturbed much by the nature of the terminal ligands. Cyclic voltammetry of **2** showed an irreversible wave corresponding to Mn(III,IV) reduction at 0.27 V versus SCE using a Pt indicator electrode. Measurement of room temperature magnetic susceptibility on powdered samples of **1** and **2** provided magnetic moments of 3.57 and 1.87 μ_B, respectively.

Table 2
Selected interatomic distances (Å) and bond angles (°) for $[Mn_2O_2(pbz)_4]^{3+}$ (1)

Distances					
Mn(1)–O(1)	1.769(10)	Mn(1)–O(2)	1.814(10)	Mn(1)–N(1)	1.981(13)
Mn(1)–N(3)	2.114(12)	Mn(1)–N(4)	2.000(12)	Mn(1)–N(6)	2.086(13)
Mn(2)–O(1)	1.794(10)	Mn(2)–O(2)	1.823(10)	Mn(2)–N(7)	1.935(13)
Mn(2)–N(9)	2.078(13)	Mn(2)–N(10)	2.009(13)	Mn(2)–N(12)	2.121(13)
Mn(1)···Mn(2)	2.729(3)				
Angles					
O(1)–Mn(1)–O(2)	81.7(5)		O(1)–Mn(1)–N(1)	92.8(5)	
O(1)–Mn(1)–N(1)	98.4(5)		O(1)–Mn(1)–N(3)	167.1(5)	
O(2)–Mn(1)–N(3)	90.2(5)		N(1)–Mn(1)–N(3)	78.4(5)	
O(1)–Mn(1)–N(4)	101.1(5)		O(2)–Mn(1)–N(4)	92.0(5)	
N(1)–Mn(1)–N(4)	163.8(5)		N(3)–Mn(1)–N(4)	89.2(5)	
O(1)–Mn(1)–N(6)	90.1(5)		O(2)–Mn(1)–N(6)	166.5(5)	
N(1)–Mn(1)–N(6)	92.6(5)		N(3)–Mn(1)–N(6)	99.7(5)	
N(4)–Mn(1)–N(6)	79.0(5)		O(1)–Mn(2)–O(2)	80.8(5)	
O(1)–Mn(2)–N(7)	103.7(5)		O(2)–Mn(2)–N(7)	92.5(5)	
O(1)–Mn(2)–N(9)	89.5(5)		O(2)–Mn(2)–N(9)	166.4(5)	
N(7)–Mn(2)–N(9)	80.5(5)		O(1)–Mn(2)–N(10)	92.0(5)	
O(2)–Mn(2)–N(10)	97.0(5)		N(7)–Mn(2)–N(10)	162.8(5)	
N(9)–Mn(2)–N(10)	92.8(5)		O(1)–Mn(2)–N(12)	169.6(5)	
O(2)–Mn(2)–N(12)	96.3(5)		N(7)–Mn(2)–N(12)	86.3(5)	
N(9)–Mn(2)–N(12)	94.9(5)		N(7)–Mn(2)–N(12)	78.5(5)	
Mn(1)–O(1)–Mn(2)	99.9(5)		Mn(1)–O(2)–Mn(2)	97.2(5)	

Table 3
Selected interatomic distances (Å) and bond angles (°) for $[Mn_2O_2(pbz)_4]^{4+}$ (2)

Distances					
Mn–O(1)	1.794(4)	Mn–O(1′)	1.802(4)	Mn–N(1)	1.980(6)
Mn–N(3)	2.106(6)	Mn–N(4)	1.957(6)	Mn–N(6)	2.095(6)
Mn···Mn′	2.724(2)				
Angles					
O(1)–Mn–N(1)	99.9(2)		O(1)–Mn–N(3)	93.9(2)	
N(1)–Mn–N(3)	79.2(2)		O(1)–Mn–N(4)	90.5(2)	
N(1)–Mn–N(4)	164.5(3)		N(3)–Mn–N(4)	88.8(2)	
O(1)–Mn–N(6)	164.9(2)		N(1)–Mn–N(6)	92.4(2)	
N(3)–Mn–N(6)	97.0(2)		N(4)–Mn–N(6)	79.3(2)	
O(1)–Mn–O(1′)	81.4(2)		N(1)–Mn–O(1′)	92.9(2)	
N(3)–Mn–O(1′)	170.0(2)		N(4)–Mn–O(1′)	100.0(2)	
N(6)–Mn–O(1′)	89.3(2)		Mn–O(1)–Mn′	98.5(2)	

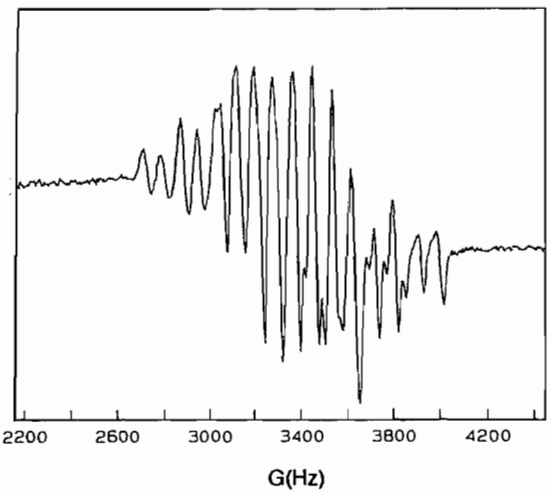

Fig. 4. The X-band EPR spectrum of $[Mn_2O_2(pbz)_4]^{3+}$ (1) in CH_3CN solution at 110 K. Conditions: microwave frequency, 9.45 GHz; microwave power 203 mW; 5 scans.

3.4. Resonance Raman spectra

Resonance Raman (RR) spectroscopy has been quite successful in structural elucidation of the oxo bridged active sites in metalloproteins and model complexes due to strong enhancements of the metal–oxygen stretching vibrations via coupling to the O→M electronic charge transfer transitions in the visible region [18]. For the centrosymmetric planar Mn_2O_2 core with D_{2h} symmetry, two Mn–O stretching modes are predicted to be Raman allowed (A_g and B_{1g}) and two to be IR active (B_{2u} and B_{3u}). Fig. 5 presents RR spectra in the 500–800 cm^{-1} region for $[Mn_2O_2(pbz)_4]^{3+}$ (1) and $[Mn_2O_2(pbz)_4]^{4+}$ (2), and their ^{18}O isotopomers obtained in KCl pellets with 488.0 (1) and 457.9 (2) nm excitation wavelengths. The spectrum of 2 shows a polarized dominant band at 693 cm^{-1} which shifts to 664 cm^{-1} on ^{18}O substitution, the position and isotope shift expected for the totally symmetric A_g vibration involving stretching of short Mn(IV)–O bonds of the Mn_2O_2 core. A similar ^{18}O sensitive band is seen in the RR spectrum of the mixed-valent complex 1. This also contains a single dominant band at 694 cm^{-1} (665 cm^{-1} in ^{18}O isotopomer), that is attributed to a predominantly Mn(IV)–O stretching mode, suggesting very

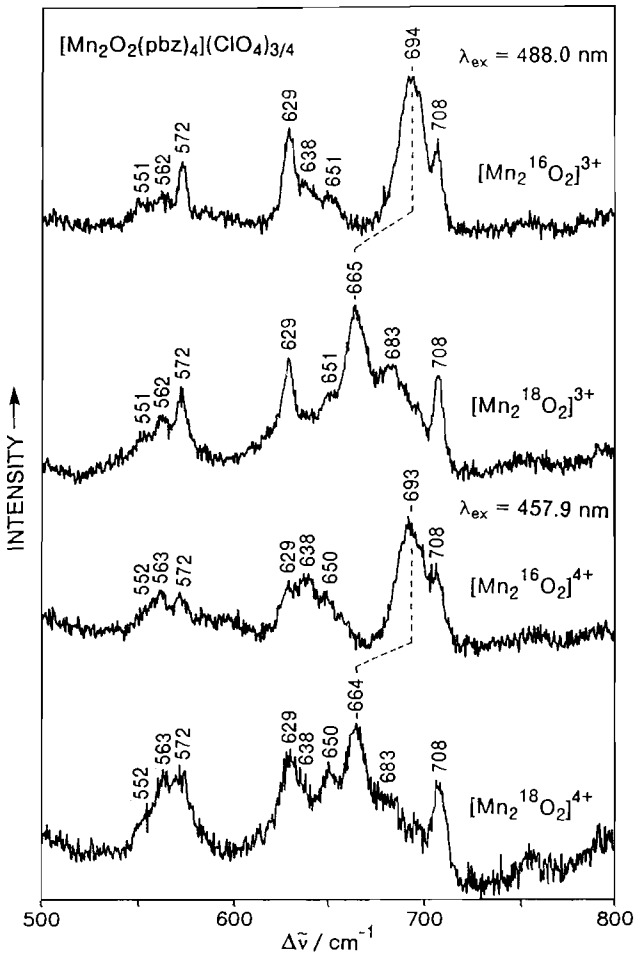

Fig. 5. RR spectra of $[Mn_2O_2(pbz)_4]^{3+}$ (**1**) and $[Mn_2O_2(pbz)_4]^{4+}$ (**2**), and their ^{18}O isotopomers obtained in KCl pellets at room temperature with 488.0 (**1**) and 457.9 (**2**) nm excitation wavelengths (100 mW) and 6 cm^{-1} slit widths. The Mn(1V)–O stretching bands are correlated.

little perturbation of the ground state geometry. A more detailed analysis of the vibrational spectra of the Mn_2O_2 cores in a series of complexes, together with ^{18}O-isotopic shifts and normal mode analysis, will be discussed elsewhere [19].

4. Conclusions

A new Mn complex containing the (di-μ-oxo)dimanganese(III,IV) mixed-valent core has been isolated, which undergoes a pH dependent disproportionation to its (di-μ-oxo)dimanganese(IV,IV) form. The minimal structural perturbations in the Mn_2O_2 core in two different oxidation states suggest the feasibility of such a core to accommodate the extra storage of positive charge without losing its structural integrity. In contrast, a similar pH dependent process with the bpy analog of **1** leads to a structural rearrangement to a trimeric $[Mn_3O_4]^{4+}$ core. Inasmuch as the Mn^{3+}/Mn^{4+} redox cycle involves minimal structural changes around the metal center, a similar mechanism can be envisioned in proteins, where a preorganized structure enforced by protein conformation facilitates electron transfer readily without a large structural rearrangement around the metal coordination center. The observed invariance of the OEC ~ 2.7 Å vector in EXAFS from S_1–S_3 states [20] implies a maintainance of the di-μ-oxo core through sequential oxidation at the metal center. Finally, the Mn(IV)–O stretching mode of the Mn_2O_2 unit can be effectively enhanced in the RR spectrum with visible excitation, which provides a useful probe in the structural characterization of Mn containing active sites involving two oxo bridges.

Acknowledgements

This work was supported by the National Institutes of General Medical Sciences, NIH (GM-48370). Receipt of a Robert A. Welch Foundation predoctoral fellowship (to B.C.D.) is gratefully acknowledged. In addition, we thank Professors C.J. Carrano (Southwest Texas State University) and G.C. Dismukes (Princeton University) for recording the magnetic measurements and low-temperature (liq. He) EPR spectra, respectively. We also express thanks to Dr J. Korp (University of Houston) for assistance in solving the crystal structures of **1** and **2**, and to one of the reviewers for suggesting the reaction pathway shown in Scheme 1(b).

References

[1] (a) V.L. Pecoraro, *Photochem. Photobiol., 48* (1988) 249; (b) G.W. Brudvig and R.H. Crabtree, *Prog. Inorg. Chem., 37* (1989) 99; (c) J.B. Vincent and G. Christou, *Adv. Inorg. Chem., 33* (1989) 197; (d) K. Wieghardt, *Angew. Chem., Int. Ed. Engl., 28* (1989) 1153; (e) L. Que, Jr. and A.E. True, *Prog. Inorg. Chem., 38* (1990) 98; (f) H.H. Thorp and G.W. Brudvig, *New J. Chem., 15* (1991) 479.

[2] (a) Y. Kono and I. Fridovich, *J. Bacteriol., 155* (1983) 742; (b) *J. Biol. Chem., 258* (1983) 6015; (c) W.F. Beyer, Jr. and I. Fridovich, *Biochemistry, 24* (1985) 6460; (d) R.M. Fronko, J.E. Penner-Hahn and C.J. Bender, *J. Am. Chem. Soc., 110* (1988) 7554; (e) G.S. Waldo, R.M. Fronko and J.E. Penner-Hahn, *Biochemistry, 30* (1991) 10486; (f) G.S. Waldo, S. Yu and J.E. Penner-Hahn, *J. Am. Chem. Soc., 114* (1992) 5869; (g) J.E. Penner-Hahn, in V.L. Pecoraro (ed.), *Manganese Redox Enzymes,* VCH, New York, 1992, p. 29; (h) V.V. Barynin and A.I. Grebenko, *Dokl. Akad. Nauk. SSSR, 286* (1986) 461; (i) V.V. Barynin, A.A. Vagin, V.R. Melik-Adamyan, A.I. Grebenko, S.V. Khangulov, A.N. Popov, M.E. Andrianova and B.K. Vainshtein, *Dokl. Akad. Nauk. SSSR, 288* (1986) 877; (j) S.V. Khangulov, V.V. Barynin and S.V. Antonyuk-Barynina, *Biochim. Biophys. Acta, 1020* (1990) 25.

[3] (a) G.C. Dismukes, *Photochem. Photobiol., 43* (1986) 99; (b) G.T. Babcock, in J. Amesz (ed.), *New Comprehensive Biochemistry: Photosynthesis,* Elsevier, New York, 1987, p. 125; (c) G. Renger, *Photosynthetica, 21* (1987) 203; (d) *Angew. Chem., Int. Ed. Engl., 26* (1987) 643; (e) A.W. Rutherford, *Trends*

Biochem. Sci., 14 (1989) 227; (f) A.G. Volkov, *Bioelectrochem. Bioenerg., 21* (1989) 3; (g) G.W. Brudvig, W.F. Beck and J.C. de Paula, *Annu. Rev. Biophys. Biophys. Chem., 18* (1989) 25; (h) D.F. Ghanotakis, C.F. Yocum, *Annu. Rev. Plant. Physiol. Plant Mol. Biol., 41* (1990) 255; (i) O. Hansson and T. Wydrzynski, *Phosynth. Res., 23* (1990) 131.

[4] (a) P. Joliot, G. Barbieri and R. Chabaud, *Photochem. Photobiol., 10* (1969) 309; (b) B. Kok, B. Forbush and M. McGloin, *Photochem. Photobiol., 11* (1970) 457.

[5] (a) V. Forster and W. Junge, *Photochem. Photobiol., 41* (1985) 183; (b) O. Saygin and H.T. Witt, *Photobiochem. Photobiophys., 10* (1985) 71.

[6] G.C. Dismukes and P. Mathis, *FEBS Lett., 178* (1984) 51.

[7] S. Menage, J.-J. Girerd and A. Gleizes, *J. Chem. Soc., Chem. Commun.,* (1988) 431.

[8] B.C. Dave, R.S. Czernuszewicz, M.R. Bond and C.J. Carrano, *Inorg. Chem., 32* (1993) 3593.

[9] (a) H.H. Thorp, J.E. Sarneski, G.W. Brudvig and R.H. Crabtree, *J. Am. Chem. Soc., 111* (1989) 9249; (b) H.H. Thorp, E.F. Bowden and G.W. Brudvig, *J. Electroanal. Chem., 290* (1991) 293; (c) R. Manchanda, H.H. Thorp, G.W. Brudvig and R.H. Crabtree, *Inorg. Chem., 30* (1991) 494.

[10] S. Pal, M.K. Chan and W.H. Armstrong, *J. Am. Chem. Soc., 114* (1992) 6398.

[11] (a) P.M. Plaskin, R.C. Stoufer, M. Mathew and G. Palenik, *J. Am. Chem. Soc., 94* (1972) 2121; (b) S.R. Cooper and M. Calvin, *J. Am. Chem. Soc., 99* (1977) 6623; (c) S.R. Cooper, G.C. Dismukes, M.P. Klein and M. Calvin, *J. Am. Chem. Soc., 100* (1978) 7248.

[12] J.E. Sarneski, H.H. Thorp, G.W. Brudvig, R.H. Crabtree and G.K. Schulte, *J. Am. Chem. Soc., 112* (1990) 7255.

[13] (a) R.S. Czernuszewicz, *Appl. Spectrosc., 40* (1986) 571; (b) in C. Jones, B. Mulloy and A.H. Thomas (eds.), *Methods in Molecular Biology,* Vol. 17, Humana, Totowa, NJ, 1993, p. 345.

[14] (a) W.H. Armstrong and S.J. Lippard, *J. Am. Chem. Soc., 106* (1984) 4632; (b) P. Knopp and K. Wieghardt, *Inorg. Chem., 30* (1991) 4061; (c) C.J. Carrano, R. Verastague and M.R. Bond, *Inorg. Chem., 32* (1993) 3589.

[15] (a) K.S. Hagen, T.D. Westmoreland, M.J. Scott and W.H. Armstrong, *J. Am. Chem. Soc., 111* (1992) 1907; (b) E.J. Larson, P. Riggs, J.E. Penner-Hahn and V.L. Pecoraro, *J. Chem. Soc., Chem. Commun.,* (1992) 102; (c) J.M. Carroll and J.R. Norton, *J. Am. Chem. Soc., 114* (1992) 8744.

[16] M. Stebler, A. Ludi and H.-B. Burgi, *Inorg. Chem., 25* (1986) 4743.

[17] G.C. Dismukes, J.E. Sheats, P. Mathur and R.S. Czernuszewicz, in M. Baltscheffsky (ed.), *Current Research in Photosynthesis,* Vol. 1, Kluwer, Dordrecht, Netherlands, 1990, p. 773.

[18] J. Sanders-Loehr, in L. Que, Jr. (ed.), *Metal Clusters in Proteins,* ACS Symposium Series 372, American Chemical Society, Washington, DC, 1988, p. 49.

[19] B.C. Dave and R.S. Czernuszewicz, manuscript in preparation.

[20] (a) G.N. George, R.C. Prince and S.P. Cramer, *Science, 243* (1989) 789; (b) R.D. Guiles, J.-L. Zimmermann, A.E. Mcdermott, V.K. Yachandra, J.I. Cole, S.L. Dexheimer, R.D. Britt, K. Wieghardt, U. Bossek, K. Sauer and M.P. Klein, *Biochemistry, 29* (1990) 471; (c) J.E. Penner-Hahn, R.M. Fronko, V.L. Pecoraro, C.F. Yocum, S.D. Betts and N.R. Bowlby, *J. Am. Chem. Soc., 112* (1990) 2549; (d) K. Sauer, V.K. Yachandra, R.D. Britt and M.P. Klein, in V.L. Pecoraro (ed.), *Manganese Redox Enzymes,* VCH, New York, 1992, p. 141; (e) M.P. Klein, V.K. Yachandra, V.J. DeRose, I. Mukerji, M.J. Latimer and K. Sauer, *J. Inorg. Biochem., 43* (1991) 363.